Macromolecular Rapid Communications
www.mrc-journal.de

Superhydrophobic and Anti-Icing Coatings Made of Hierarchically Nanofibrillated Polymer Colloids

*Austin H. Williams, Sangchul Roh, Yosra Kotb, and Orlin D. Velev**

The deposition of coatings with hierarchical morphology from hydrophobic and hydrophilic polymers is a common approach for making superhydrophobic and superhydrophilic coatings. The water-repellent, water-wicking, and anti-icing coatings reported here are made from a class of materials called soft dendritic colloids (SDCs). The branched, nanofibrous SDCs are produced in suspension through nonsolvent-induced phase separation in a turbulent medium. The properties of coatings formed by drying ethanol suspensions of SDCs made of polystyrene, polyvinyl alcohol, and polyester are compared. The highly branched SDC morphology creates entangled, porous coating layers with strong physical adhesion to the substrate due to the multitude of nanofiber sub-contacts analogous to the "gecko leg effect". Polystyrene SDC coatings show excellent superhydrophobicity but weaker adhesion due to low surface energy. Alternatively, polyvinyl alcohol SDC coatings show superhydrophilicity and strong adhesion from their high surface energy. Two strategies to improve the adhesivity and cohesivity of the SDCs layers are shown effective – use of intertwined networks and of silicone droplet microbinders. The water repulsion, together with the air trapped in the blended superhydrophobic coatings also makes them effective against ice nucleation and adhesion. Finally, these SDCs make thin, flexible, and durable nonwovens with similar properties.

1. Introduction

The engineering of surfaces with advanced wetting, self-cleaning, anti-corrosive, and anti-icing properties has been a topic of intense research interest and thrust to applications.[1–4] The research studies aimed to produce superhydrophobic surfaces have focused on reducing the surface energy of the substrate, as well as achieving the high degree of surface roughness to trap air pockets between the water droplet and the surface and suspend the droplets into a Cassie-Baxter state.[5–7] Polymeric coatings seeking to mimic the "lotus leaf effect" by having low surface energies and hierarchical surface roughness typically are produced by microphase separation, sol-gel processes, or electrospinning. Such coatings commonly achieve superhydrophobicity with apparent water contact angles (WCA) greater than 150° and low tilt angles less than 5° that promote water droplet roll-off.[8–12]

A common strategy in the related field of fabricating coatings with anti-icing properties has been to utilize similar hierarchical superhydrophobic surface architectures to reduce ice accumulation by decreasing the contact area between the surface and impinging water droplets. This allows to decrease the thermal conduction between the surface and the droplet that leads to heterogeneous ice nucleation.[13–20] Coating architectures with hierarchical features both on the micro- and nano-scales have been found to maximize liquid repellency, facilitate droplet roll-off, delay ice nucleation in static water droplets, and, in some cases, reduce ice adhesion strength.[21–34] Chemically modified polymeric anti-icing coatings are often limited in their scalability and can be subject to fouling of the coating or mechanical abrasion, which leads to reduced functionality.[35] One common strategy to mitigate such deterioration is to create thicker, porous coatings from polymers with low surface energy as opposed to functionalizing a thin hydrophobic layer on the surface. Such coatings are resilient to mechanical abrasion and exfoliation because the removal of a thin surface layer reveals more underlying hydrophobic material and thus the coatings maintain superhydrophobicity.[36,37]

Here, we present several novel classes of nanofibrous polymeric coatings, and porous nanofibrous sheets, made of soft dendritic colloids (SDCs). SDCs are a hierarchically structured polymer nanomaterial with a micrometer-sized backbone, surrounded by branched fibers spanning up to three orders of magnitude in diameter.[38] A major advantage to utilizing SDCs compared to simple nanofibers produced by other methods is that SDCs are inherently hierarchical fibrillar material that is produced in suspension, which can be easily coated as opposed to fibers confined into a 2D mat. As we show, dispersing the SDCs

A. H. Williams, S. Roh, Y. Kotb, O. D. Velev
Department of Chemical and Biomolecular Engineering
North Carolina State University
Raleigh, NC 27695, USA
E-mail: odvelev@ncsu.edu

The ORCID identification number(s) for the author(s) of this article can be found under https://doi.org/10.1002/marc.202200513

DOI: 10.1002/marc.202200513

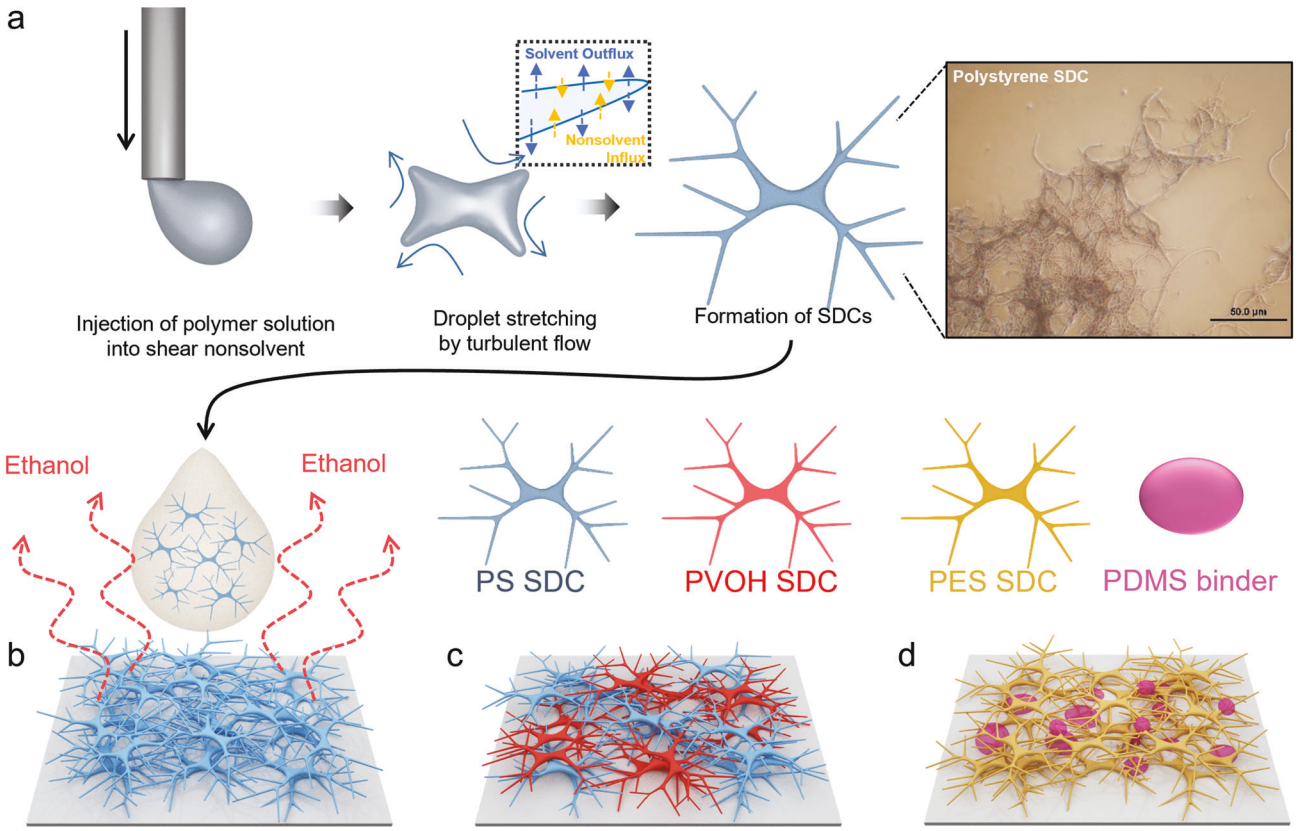

Figure 1. Schematics of SDC coatings making and structure. a) Diagrams illustrating SDC manufacture, re-suspension in alcohol, and the casting of b) pure SDC, c) bicontinuous network SDC, and d) SDC/binder composite surface coatings.

in a volatile medium such as ethanol (EtOH) enables the facile casting of that suspension on any surface. After the evaporation of the EtOH medium, SDC suspension casting results in the robust formation of highly porous and nanofibrous surface coatings (**Figure 1**). The characteristic branched fibrillar morphology of the SDCs results in a robust, self-assembled adhesive network due to an adhesive mechanism analogous to the contact-splitting phenomenon exhibited by the legs of gecko lizards. The solvent evaporation deposition process allows the SDC fibers to conform to a substrate regardless of its topography. Due to the combination of the contact splitting effect and omnipresent van der Waals interactions,[38] the SDCs in these coatings also adhere to substrates with little effect of the polymer's composition and surface energy, and the surface's topography and surface energy.

2. Results and Discussion

We show that SDC coatings can be prepared from a range of polymers of varying chemical compositions and that the wetting properties and mechanical characteristics of the SDC coating are dependent on the polymer comprising the SDCs. The topographically overlapping multiscale fibers, inherent to SDC coatings, amplify the hydrophobicity or hydrophilicity of the surface coated with SDCs made from hydrophobic and hydrophilic polymers, respectively. SDC coatings comprised of hydrophobic polymers also exhibit anti-icing properties, however, superhydrophobic SDC coatings and nonwovens composed of a single polymer have relatively poor mechanical properties. To mitigate the inherent inverse relationship between high mechanical integrity and superhydrophobicity, we evaluated two strategies to improve the SDC coating properties: 1) formation of bicontinuous SDC networks, and 2) adding an emulsified, elastomeric polydimethylsiloxane (PDMS) binder.

2.1. Wetting Properties of SDC Coatings

The SDC coatings from polystyrene (PS), polyvinyl alcohol (PVOH), and polyester (PES) were deposited by casting on glass and metal surfaces from EtOH suspensions prepared as described in the Experimental Section. The scanning electron micrographs shown in **Figure 2** illustrate the structures of SDCs and SDC-coated glass slides from each polymer, where it is seen that the entangled fibers of adjacent SDCs form a continuous, intertwined, highly porous network on the substrate. This fibrous coating architecture results in surface topography with multiscale micro- and nano-scale features, a key characteristic of superhydrophobic and liquid-repellent surfaces.[24]

To investigate the effect of SDC surface roughness on the wetting behavior, we first measured the WCA on uniform films prepared by spin-coating composed of PS, PES, and PVOH. These data were then compared to the WCAs of SDC coatings prepared from the same polymers (**Table 1**). The large difference in the

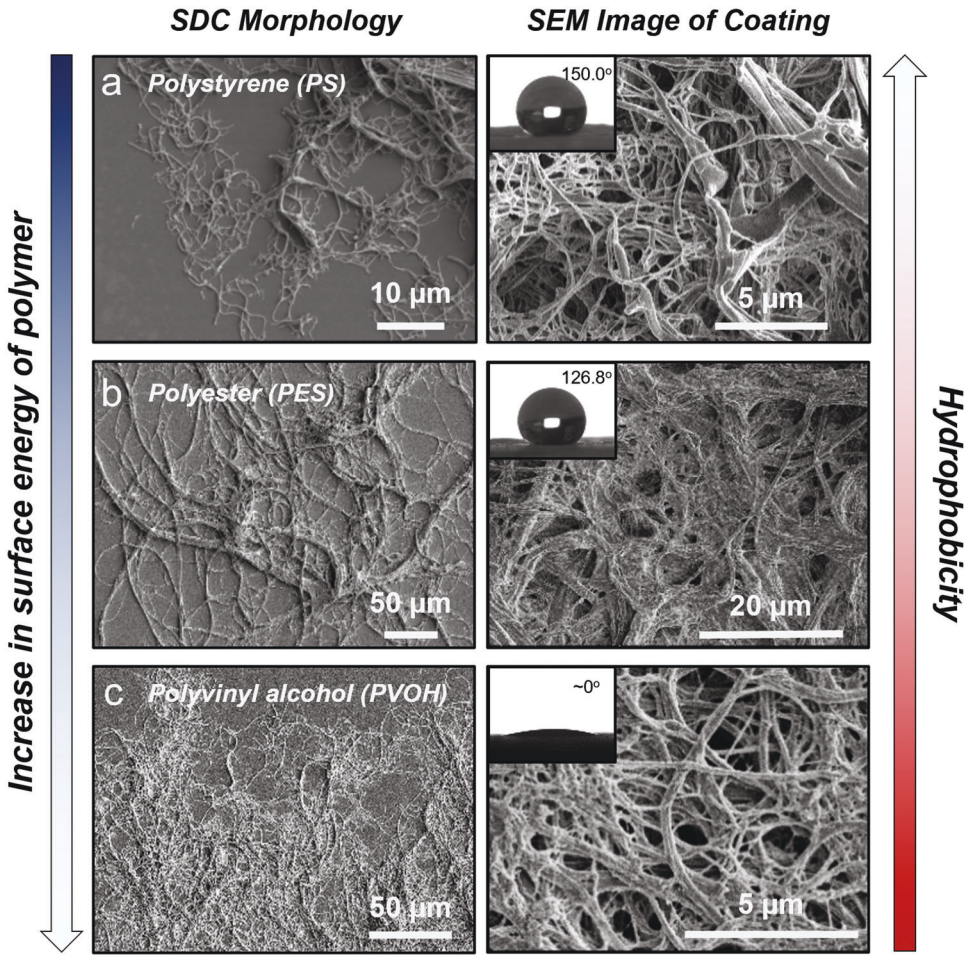

Figure 2. Microscopy of PS, PES, and PVOH SDCs and their coatings. Scanning electron micrographs of a) PS, b) PES, and c) PVOH SDCs morphology and SDC coatings with inset images showing representative water contact angle on each coating. Note that water spontaneously spreads on PVOH SDC coatings. The hierarchically branched fibers in these coatings overlap to create a highly porous continuous network.

Table 1. Summary of data for WCA on smooth films, WCA of SDC coatings of different polymers, and porosities of SDC coatings.

Polymer	Thin Film WCA [°]	SDC Coating WCA [°]	Porosity [%]
PS	100.7 ± 1.8	150.1 ± 5.0	92.49 ± 1.35
PES	75.5 ± 1.2	126.8 ± 5.7	80.47 ± 1.10
PVOH	57.4 ± 5.6	≈ 0	23.18 ± 5.07

static contact angles of water droplets on flat films and SDC coatings composed of the same polymer shows that the SDC surface topography amplifies the wetting properties of the coatings consistent with the Wenzel model.[39] Coatings from the PS and PES SDCs exhibited strongly hydrophobic behavior, while the coating from intrinsically hydrophilic PVOH SDCs was superhydrophilic, as water droplets were actively spreading after deposition.

These data were next correlated with the cohesivity and mechanical resilience of the coatings. The simplest adhesion model, the Dupré equation, describes how the work of cohesion and adhesion between two species is directly related to the surface energy of one or both materials.[40] The more hydrophobic PS and PES SDCs, which have lower surface energies, show decreased cohesion within the bulk network, and yield higher coating porosities with values over 80%. An efficient way to quantify the durability of SDC coatings is to prepare nonwoven SDC sheets. The SDC sheets were prepared by filtering SDC from EtOH suspensions onto polyvinylidene fluoride filter pads and removing the SDC layer from the filter surface after drying. SDC membrane thickness was evaluated using a micrometer and confirmed with electron microscopy. Tensile analysis was directly performed on the SDC sheets and the mechanical properties including elastic modulus and toughness of the SDC nonwovens were evaluated (**Table 2**). The mechanical properties of SDC membranes composed of different polymers can be correlated to thin, smooth polymer coatings prepared from the same polymers (Figure S1, Supporting Information). The data listed in Table 2 summarize the mechanical properties of PS, PES, and PVOH SDC nonwoven sheets.

The results of the tensile analysis of the SDC sheets show that the PS SDC network, while quite hydrophobic, is very soft with

Table 2. Mechanical properties of porous SDC sheets composed of PS, PES, and PVOH. Elastic modulus is measured in the linear elastic region of their stress-strain curve. Tensile strength is measured as tensile stress at rupture. Toughness is measured as the area under stress-strain curve prior to rupture and elongation is the strain in mm/mm at nonwoven rupture.

SDC Polymer	Modulus [Mpa]	Strength [kPa]	Toughness [kPa]	Elongation [%]
PS SDC	7.84 ± 1.16	120 ± 20	1.74 ± 0.60	2.40 ± 0.51
PES SDC	30.6 ± 14.8	277 ± 11	604 ± 113	29.8 ± 4.16
PVOH SDC	110 ± 2.22	295 ± 78	62.5 ± 39.8	3.41 ± 1.17

very low toughness. The tensile moduli of the PES and PVOH SDC nonwovens seem to follow an inverse trend with the porosities data shown in Table 1. This trend suggests that the surface energy of the material comprising SDCs determines the cohesive packing of fibers within the film and that generally, lower surface energy polymers will yield SDCs coatings with higher porosities, but with lower stiffness and toughness.[41,42] While the PVOH SDC nonwoven displays the maximum stiffness (110 ± 2.22 MPa), the PES SDC nonwoven shows greatly increased toughness (604 ± 113 kPa) compared to those of PS and PVOH. This is likely due to the PES polymer being far above its T_g of −40 °C and thus having higher elasticity at room temperature compared to the glassy PS and PVOH polymers. Pure SDC coatings are superhydrophobic, but generally demonstrate weaker adhesion to the substrate and weaker cohesion throughout the network as these SDC are composed of low surface energy polymers. This weaker fiber–fiber cohesion throughout the bulk networks renders these SDC films (e.g., from PS) more prone to mechanical abrasion. However, abrasion typically increases the superhydrophobic properties of their surfaces as the native underlying layer of SDCs is revealed. Inversely, high surface energy polymers (e.g., PVOH) form more densely packed nonwovens evidenced by lower porosity, higher elastic modulus, and superhydrophilicity.

2.2. Bicontinuous Soft Dendritic Colloid Networks

One approach that could improve and tailor the coating properties is the deposition of intertwined nanofibrous networks by mixing suspensions of SDC from different polymers in EtOH prior to coating. The properties of these "bicontinuous" coatings were investigated based on a system consisting of a blend of PS and PVOH SDCs. This polymer pair was chosen because PS SDCs show superhydrophobic behavior, but lack durability, while PVOH SDC form mechanically robust networks, albeit being hydrophilic. The electron micrograph of a bicontinuous PS/PVOH SDC (50/50 w/w) coating in **Figure 3**a (imaged on the macroscale in Figure 3b) shows that the highly entangled fibers of the two-polymer network are visually indistinguishable, which is also observed with bicontinuous SDC network regardless of the mixing ratio.

Next, we investigated the hydrophobicity of the bicontinuous PS/PVOH SDC network. In general, as the wt.% of PVOH in the SDC blend increases, theWCA gradually decreases. The decrease in the WCA is consistent with an increase in the PVOH SDCs exposed on the surface that interacted with the water droplet. Surprisingly, the coatings exhibited hydrophobicity (WCA > 90°) during inclusion of up to ≈ 50 wt.% PVOH in the SDC of the network (a decrease in the WCA from ≈150° to ≈100°), while the toughness of the membrane increased 2×. The non-linear decrease in the WCA suggests that the water droplet did not penetrate the PS/PVOH surface and the air pockets in the network, which corresponds to the Cassie-Baxter state. As a result, a water jet reaching the surface of the nonwoven gets repelled without exhibiting wetting even in the presence of a continuous PVOH network (Figure 3c,e).

The mechanical properties of the PS/PVOH SDC networks were characterized by performing tensile analysis on nonwoven sheets of the same composition. The composite PS/PVOH nonwoven blend exhibits appr. 3× higher tensile modulus and appr. 5× larger toughness than that of the PS SDC nonwoven (Figure 3f), while the elongation at break is not affected significantly (Figure S2, Supporting Information). When measured using lap shear strength testing (see Supporting Information), the PS/PVOH SDC blends exhibit adhesion trends that follow an approximately linear relationship between the adhesion values recorded for pure PS and PVOH SDCs (Figure S3, Supporting Information). Peel-off adhesion tests were performed to compare the adhesion performance of SDC coatings from PS and PS/PVOH blend. The results showed much better adhesion for the bicontinuous PS/PVOH SDC coatings, which displayed minimal damage compared to the PS SDC coatings that were largely removed from the glass substrate after peeling off (Figure S4, Supporting Information).

The strongly hydrophobic and water-repellent surface, enhanced adhesivity and cohesion, and low thermal conductance of the air-containing network suggest good anti-icing properties of these coatings. These properties were evaluated for bicontinuous SDC networks and compared to the ones of the pure polymers. First, we measured the droplet ice nucleation times, defined as the time necessary to see heterogenous ice formation completely permeate a 5 μL water droplet (exemplified in Figure 3d). These data are plotted in Figure 3e together with the apparent WCAs on these coatings determined by goniometry. The ice nucleation times decrease little until appr. 50% PVOH and then plunge towards the low values for pure PVOH SDCs. Specifically, both the apparent contact angle and the droplet freezing time values for a coating composition of 75/25 (w/w) PS/PVOH SDCs are nearly the same as those of the pure PS SDC coating. However, at this composition, the adhesion of the coating measured by lap shear strength increased nearly 50% compared to that of PS SDCs alone. Overall, the blended PS/PVOH SDC coating network combines good water repellency and ice retardation properties, while also gaining much improved mechanical integrity due to the incorporation of PVOH SDCs into the SDC network (Figure 3f).

The second parameter determining the anti-icing abilities of these coatings is the ice adhesion strength. The strengths of ice adhesion to SDC and SDC composite coatings were determined by a common method described previously (Figure S5, Supporting Information).[42–44] As the pure PS SDC coating showed low resiliency, the removal of the ice mold from these samples resulted in serious coating damage and in some cases tearing off from the aluminum substrate (labeled as adhesive failure). The pure PVOH SDC coating had both increased (unfavorable) ice adhesion and nucleation rate as the spread-out droplet had a large

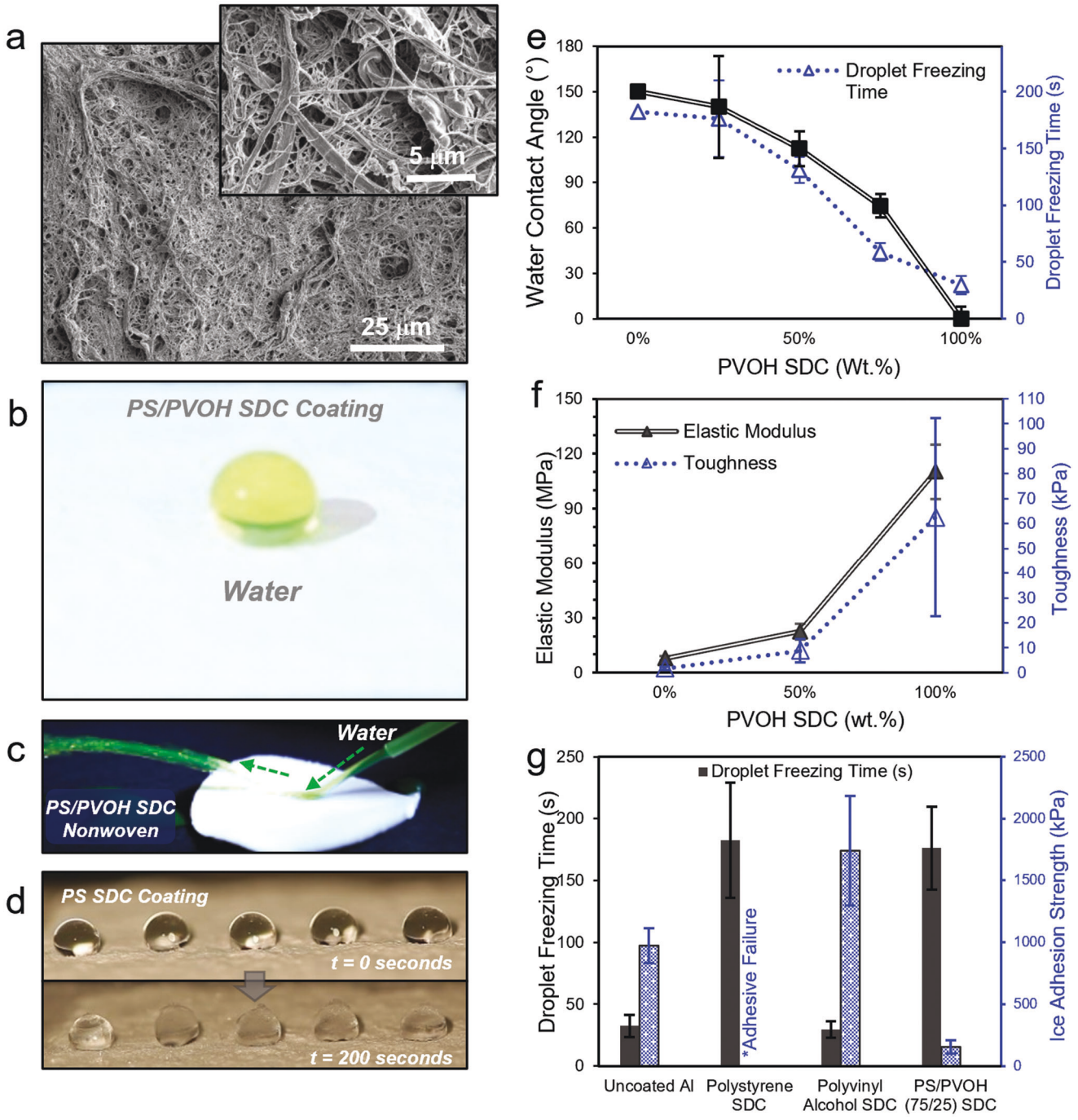

Figure 3. Wetting and anti-icing properties of PS/PVOH bicontinuous SDC coatings. a) SEM images of a PS/PVOH (50/50) blended SDC coating. b) Picture of a PS/PVOH (75/25) SDC coating. c) Demonstration of water repellency of a PS/PVOH (75/25) SDC nonwoven. d) Examples of heterogeneous ice nucleation of 5 μL water droplets on a PS SDC coated Al substrate. e) Apparent contact angle (black) and droplet freezing time (blue) versus. PS wt.% for PS/PVOH bicontinuous networks of 2 mg cm^{-2} ($n = 10$). f) Elastic modulus and toughness of PS/PVOH SDC nonwovens of varying composition. g) Droplet freezing time (black) and ice adhesion strength (blue) for aluminum, PS, PVOH, and PS/PVOH SDC coatings of 2 mg cm^{-2} ($n = 10$).

contact area with the cooled substrate. However, the continuous composite PS/PVOH (75/25 w/w) SDC coating showed an ice nucleation time consistent with the pure PS coating but exhibited ≈ 5× reduction in ice adhesion strength (≈200 kPa) compared to the aluminum substrate control (Figure 3g). Moreover, the bicontinuous SDC coating layer remained intact unlike what we observed with pure PS SDC, indicating that these coatings possess sufficient mechanical integrity.

As shown in Figure S6, Supporting Information, the detached ice mold also removed pieces from the surface of the PS SDC

coating while there were minimal traces of the PS/PVOH (75/25) coating removed demonstrating the superior durability of the PS/PVOH coating after ice removal. Thus, this balanced bicontinuous SDCs composition possessed the best properties of the studied systems. Notably, for both coatings, the eroded area where the ice was removed did not show any visible change in the underlying SDC morphology, demonstrating that these coatings can shed off their surface layers and still retain their porosity and repellency after ice removal ("ablative" protection, Figure S6e, Supporting Information).

2.3. Polydimethylsiloxane Microdroplet Binder for SDC Coatings

Next, we investigated in more detail the use of PDMS binder with SDCs. The addition of an elastomeric binder has previously been shown to improve the hydrophobic and mechanical properties of nanofibrous 3D networks and has previously found application as icephobic coatings and nonwovens.[29–31,45–47] To explore SDC networks that might exhibit hydrophobic and anti-icing properties well-suited for applications requiring a more durable, yet porous, polymer material,[31,33] we chose to investigate PES SDCs and PES SDC/PDMS composites. PES SDCs nonwovens are highly elastic and exhibit good mechanical integrity as nonwovens evidenced by their being rolled cylindrically, folded, and bent while exhibiting high WCAs (>125°) (illustrated by the images in **Figure 4**a,b) While PS SDC sheets can similarly be handled, rolled, and folded, their decreased inter-fiber adhesion in the bulk network is more easily fractured with the application of tensile stress compared to PES and PVOH nonwovens (Figure 1).

We found that the addition of PDMS slightly decreased the apparent WCA of the PES/PDMS SDC coatings, but the contact angle hysteresis (CAH) of the composite coating reached a minimum at 30 wt.% PDMS (Figure 4e). Because PDMS (WCA ≈ 90°) is slightly more hydrophobic than the continuous PES film (WCA = 75.5 ± 1.2°), we hypothesize that at low concentrations, the PDMS microdroplets within the SDC matrix decrease the average surface energy of the heterogeneous coating, but also incrementally reduce the surface roughness created by the overlapping SDC fibers. The scanning electron micrographs shown in Figure 4c-d demonstrate that as the PDMS concentration in the coating increases, small PDMS droplet moieties appear distributed at the fiber-fiber junctions and fiber-substrate interfaces. We hypothesize that at higher PDMS droplet binder concentrations, the roughness impaired by the elastomeric binder droplets adds to the roughness of the SDC fibers, so that the CAH begins to increase with greater binder concentrations beyond its minimum value seen at 30 wt.% PDMS (Figure 4e). A low CAH has been shown to be a design parameter indicator for surfaces with low ice adhesion strengths,[6] so the anti-icing properties of the formulation with 30 wt.% PDMS binder were investigated further.

In the evaluation of the anti-icing properties, the pure PES SDC coating demonstrated ≈3× increase in the droplet freezing time compared to the uncoated aluminum control but resulted in only a minor reduction in ice adhesion strength. However, the PES/PDMS composite showed greatly prolonged droplet freezing times and decreased ice adhesion strength (≈400 kPa) compared to any SDC coating composed of a single polymer. The increase in droplet freezing time with the mass (and thus, thickness) of the deposited PES and PS SDC coatings was approximately linear (Figure S7, Supporting Information), with PS SDCs showing a more efficient anti-icing effect by significantly delaying water droplet freezing times. This suggests that SDC coatings exhibit good anti-icing properties through both hydrophobic and insulation effects, as heat flow through the highly porous PS and PES SDC coatings (Table 1) would be greatly reduced, with the more porous PS SDC coating displaying a greater reduction than the PES SDC coating.

3. Conclusions

We report here the wetting behavior and anti-icing potential of SDC coatings and nonwovens composed of polymers of different chemical compositions. The hierarchically branched fibrous morphology of the SDCs allows them to physically adhere strongly to nearly any surface regardless of its topography. The SDC networks also display strong cohesion, making possible the scalable production of surface coatings and nonwovens from an enormous library of polymer materials. We show that the hierarchical morphology of the SDC coatings also amplifies their wetting properties depending on the surface energy of the polymer comprising the SDCs, due to the surface roughness granted by the overlapping fibers. This is consistent with other reports exploring how lower surface energy micro- and nano-fibrous polymer networks result in strongly hydrophobic SDC surfaces with higher porosity.[18,19] Correspondingly, higher surface energy polymers produce superhydrophilic SDC coatings with high wettability, which immediately wick away water droplets from their surfaces.

The higher surface energy of the hydrophilic SDC coatings enables higher toughness and resistance to mechanical abrasion. However, the lower surface energy of the SDCs in the superhydrophobic coatings limits their adhesion strength, and coatings of purely hydrophobic SDCs are relatively soft and amenable to abrasion. We demonstrate how this inherent challenge can be mitigated by two design strategies – making either bicontinuous SDC coatings comprised of a blend of polymer SDCs, or the addition of an elastomeric binder in the form of microdroplets. Concurrently, we show that both pure SDC and composite SDC coatings show anti-icing properties,[44] namely, increased ice nucleation time due to reduced contact area, reduced heat transfer from the surface to the droplet, and decreased ice adhesion strength. While the PS SDC coating suffered partial removal by sticking to the ice interface, it has ablative properties and could potentially resist multiple ice adhesion and removal cycles, which is additionally improved by the better adhesion and consolidation in the case of mixed PS/PVOH SDC composites.

The highly hydrophobic surfaces also demonstrate enhanced droplet bounce and roll-off. While we have focused in this study on select polymers for SDC fabrication, the technique of shear-driven polymer precipitation can readily be expanded further to produce novel nanostructured SDCs from more polymer types (e.g., polyurethane, polyvinylidene fluoride,[48] polyvinylidene fluoride-co-hexafluoropropylene, alginate,[49] chitosan and polyacrylonitrile), the principles discussed here provide insights into the choice of polymer(s) and composites that could be used

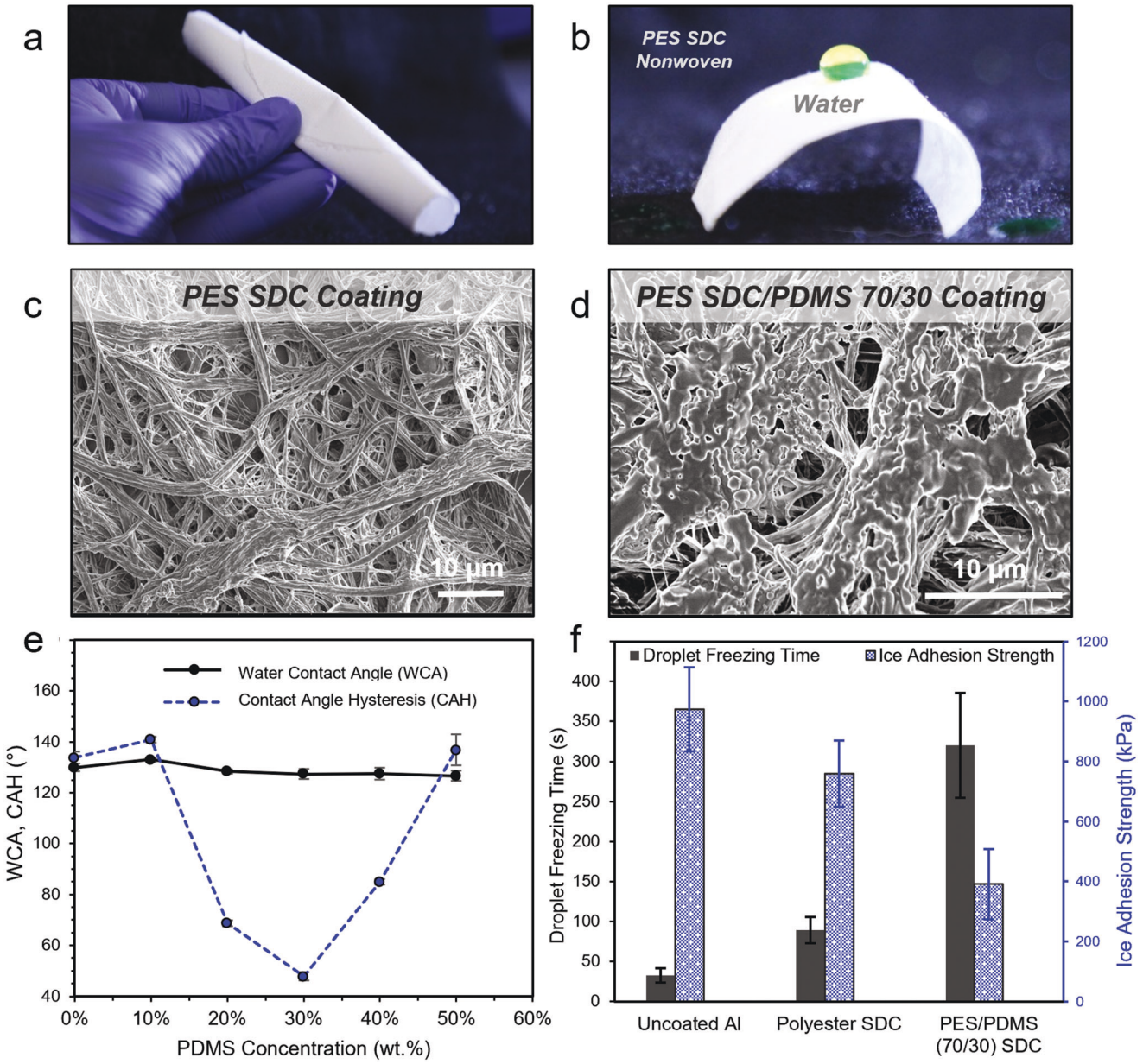

Figure 4. Wetting and anti-icing properties of PES SDC/PDMS composite coatings. a) Pictures of PES SDC membranes. b) Pictures of water droplets on a PES/PDMS coating. c) PES SDC/PDMS (70/30 w/w) coating, and d) PES SDC coating scanning electron micrographs. e) Static WCA and contact angle hysteresis on PES SDC/PDMS coatings of varying composition ($n = 5$). f) Droplet freezing time and ice adhesion strength for uncoated aluminum, a PES SDC coating, and a PES SDC/PDMS (70/30) composite coatings (2 mg cm^{-2}, $n = 5$).

to make SDC coatings with tailored surface properties and enhanced mechanical stability.

Some previously reported nanofiber coatings (typically made by electrospinning) achieve improved superhydrophobic and anti-icing performance through the incorporation of nanoparticles in the fibers.[50–52] While that approach was not investigated here, the shear-driven precipitation technique can easily achieve facile incorporation of nanoparticles into nanofibers[53] and could be used to make composite SDCs containing hydrophobic and/or ceramic nanoparticles by dispersing them in the polymer injection solution. Other potential advantages of the SDC coatings are that they can ablatively tolerate some degree of abrasion and surface exfoliation without deterioration (and even with potential regeneration) of their properties, as the SDC material in the bulk of the thick coating is chemically and morphologically identical to that at the surface.[39] Ultimately, the outstanding and highly controllable wetting and anti-icing properties of SDCs, combined with the scalability of their production, and the large library of different polymer chemistries from which SDCs can be fabricated, may enable the fabrication of a multitude of high-performance SDC coatings for both large-scale and specialty applications.

4. Experimental Section

SDC Fabrication and Coating Casting: SDCs from PS (Sigma-Aldrich, M_w = 230 kDa), PES (Eastman Ecdel 9966), and PVOH (Mowiol 18–88, 100 kDa) were fabricated using the polymers, solvents, and nonsolvents systems listed in Table S1, Supporting Information. PVOH SDCs were further cross-linked with glutaraldehyde following suspension in acetone to render them insoluble in water (Supporting Information). Following fabrication, the resulting SDCs were centrifuged at 3.0 rcf for 2 min to form a concentrated pellet, the supernatant was discarded, and the SDCs were resuspended in EtOH (Koptec) to 8× the pellet volume. This procedure was repeated 3× to remove the remaining nonsolvent from the dispersion. SDC coatings were prepared by first suspending PS, PES, or PVOH SDCs in EtOH at a concentration of 1.0 wt.%. At this concentration, the SDC suspensions begin to show yield stress behavior and gel due to fibrous entanglements between SDC particulates.[38,50] To create a SDC coating, the SDC suspensions in EtOH were evenly cast over the substrate and dried in a 50 °C oven for 24 h to remove the EtOH dispersion medium. SDC coatings of thickness 20–500 µm were cast by diluting or concentrating the SDCs in EtOH before casting.

Polydimethylsiloxane Binder for SDC Coatings: PDMS/SDC composite coatings were prepared by mixing PDMS (Sylgard 184) base with its curing agent (10:1 ratio) and leaving it at room temperature for 10 min before emulsifying the PDMS in EtOH at (1 wt.% PDMS) using a 1 cm stir bar at 1200 rpm. Immediately prior to casting, the PDMS emulsion was added to the 1.0 wt.% SDC suspension in EtOH, mixed for 1 min using a Vortex mixer and cast onto the substrate. The drying process at 50°C served to both remove the alcohol medium and cure the PDMS microdroplets within the composite. Coating thickness was determined by removing the coating with a razor blade and measuring the thickness using a handheld micrometer (Marathon).

WETTING and Anti-Icing Properties of SDC Coatings: Contact angle measurements were determined by dispensing 10 µL water droplets using a goniometer (First Ten Angstroms). CAH was calculated by subtracting the receding from the advancing contact angles measured by adding and removing water from the deposited droplet and video analysis of the contact angles by First Ten Angstroms software. Ice nucleation times were calculated by depositing 10 µL of Milli-Q water onto substrates equilibrated on a ≈10 °C Peltier plate (Linkam PE-94), videotaping the droplet nucleation process, and using image analysis to measure heterogenous ice nucleation time. Ice adhesion strengths were calculated by adopting a previously developed procedure in which hydrophobic polypropylene tips (Fisherbrand 0.1–10 mL, 4 mm diameter, 50 µL water) were utilized as ice molds. Following deposition of water into the molds, SDC coatings on aluminum substrates were placed on the Peltier plate maintained at -10 °C for 10 min. Adhesion strength was determined by attaching a force gauge (HF-30N) to a modified syringe pump (NE-4000) and removing the ice mold at a speed of 0.5 mm s^{-1}. The ice adhesion strength with calculated by Equation 1, where P_{ad} is the adhesion strength and d is the diameter of the ice mold.[40]

$$P_{ad} = \frac{4F_{ad}}{\pi d^2} \quad (1)$$

Microscopy of SDC Coatings: Optical microscopy (BX-61, Olympus) and field emission scanning electron microscopy (Verios 460L, FEI) were performed to visualize particle and coating structures. Electron microscopy was performed after sputter coating 7 nm of a gold/palladium alloy on the surface of the SDC or coating.

SDC Sheet Formation for Mechanical Analysis: One useful method of comparing the durability and toughness of SDC coatings is forming a mechanically robust and porous sheet from the SDC matrix comprising the coating. This was achieved by filtering SDC suspensions in EtOH onto a polyvinylidene fluoride filter (0.45 µm, Durapore). Once filtered, SDC sheets were dried for 24 h at 50 °C to remove residual EtOH and were cut into 10 mm wide strips. The mechanical properties of the nonwovens were then measured using a common testing machine (Instron 5943) with a crosshead speed of 5 mm min^{-1}.

Supporting Information

Supporting Information is available from the Wiley Online Library or from the author.

Acknowledgements

This study was supported by grants from US National Science Foundation, CMMI-1825476 and partially EFMA-2029327. Authors thank Dr. Michael Dickey for use of mechanical testing and goniometer instruments.

Conflict of Interest

The authors declare no conflict of interest.

Data Availability Statement

The data that support the findings of this study are available in the supplementary material of this article.

Keywords

anti-icing, nanofibers, nonwovens, soft dendritic colloids, superhydrophobic coatings

Received: June 22, 2022
Revised: August 5, 2022
Published online:

[1] I. Sas, R. E. Gorga, J. A. Joines, K. A. Thoney, *J. Polym. Sci., Part B: Polym. Phys.* **2012**, *50*, 824.
[2] R. M. Fillion, A. R. Riahi, A. Edrisy, *Renewable Sustainable Energy Rev.* **2014**, *32*, 797.
[3] M. Nosonovsky, B. Bhushan, *Curr. Opin. Colloid Interface Sci.* **2009**, *14*, 270.
[4] T. Darmanin, F. Guittard, *J. Mater. Chem. A* **2014**, *2*, 16319.
[5] J. Ai, Z. Guo, *Chem. Commun.* **2019**, *55*, 10820.
[6] A. J. Meuler, J. D. Smith, K. K. Varanasi, J. M. Mabry, G. H. McKinley, R. E. Cohen, *ACS Appl. Mater. Interfaces* **2010**, *2*, 3100.
[7] H. Wang, G. He, Q. Tian, *Appl. Surf. Sci.* **2012**, *258*, 7219.
[8] L. Cao, A. K. Jones, V. K. Sikka, J. Wu, D. Gao, *Langmuir* **2009**, *25*, 12444.
[9] N. Nuraje, W. S. Khan, Y. Lei, M. Ceylan, R. Asmatulu, *J. Mater. Chem. A* **2013**, *1*, 1929.
[10] I. Yilgor, S. Bilgin, M. Isik, E. Yilgor, *Polymer* **2012**, *53*, 1180.
[11] Y. Lin, H. Chen, G. Wang, A. Liu, *Coatings* **2018**, *8*, 208.
[12] W. Luo, J. Xu, G. Li, G. Niu, K. W. Ng, F. Wang, M. Li, *Langmuir* **2022**, *38*, 7129.
[13] H. J. Ensikat, P. Ditsche-Kuru, C. Neinhuis, W. Barthlott, *Beilstein J. Nanotechnol.* **2011**, *2*, 152.
[14] B. L. Feng, S. H. Li, Y. S. Li, H. J. Li, L. J. Zhang, J. Zhai, Y. L. Song, B. Q. Liu, L. Jiang, L. Feng, S. H. Li, Y. S. Li, H. J. Li, L. J. Zhang, J. Zhai, Y. L. Song, B. Q. Liu, L. Jiang, D. B. Zhu, *Adv. Mater.* **2002**, *14*, 1857.
[15] L. Gao, T. J. McCarthy, *Langmuir* **2009**, *25*, 14105.
[16] J. Lv, Y. Song, L. Jiang, J. Wang, *ACS Nano* **2014**, *8*, 3152.
[17] Z. Pan, F. Cheng, B. Zhao, *Polymers* **2017**, *9*, 32.
[18] P. K. Szewczyk, D. P. Ura, S. Metwally, J. Knapczyk-Korczak, M. Gajek, M. M. Marzec, A. Bernasik, U. Stachewicz, *Polymers* **2018**, *11*, 34.

[19] F. L. Huang, Q. Q. Wang, Q. F. Wei, W. D. Gao, H. Y. Shou, S. D. Jiang, *eXPRESS Polym. Lett.* **2010**, *4*, 551.
[20] T. Wang, Z. Wang, *Langmuir* **2022**, *38*, 9073.
[21] P. Eberle, M. K. Tiwari, T. Maitra, D. Poulikakos, *Nanoscale* **2014**, *6*, 4874.
[22] M. A. Sarshar, D. Song, C. Swarctz, J. Lee, C.-H. Choi, *Langmuir* **2018**, *34*, 13821.
[23] A. K. Metya, J. K. Singh, F. Müller-Plathe, *Phys. Chem. Chem. Phys.* **2016**, *18*, 26796.
[24] S. Milles, M. Soldera, B. Voisiat, A. F. Lasagni, *Sci. Rep.* **2019**, *9*, 1.
[25] Z. Zhu, Y. Tian, Y. Liu, K. Fu, Q. Chen, B. Zhang, H. Zhang, Q. Zhang, *Colloids Surf. A* **2022**, *641*, 128562.
[26] J. Liu, C. Zhu, K. Liu, Y. Jiang, Y. Song, J. S. Francisco, X. C. Zeng, J. Wang, *Proc. Natl. Acad. Sci. USA* **2017**, *114*, 11285.
[27] G. Bai, D. Gao, Z. Liu, X. Zhou, J. Wang, *Nature* **2019**, *576*, 437.
[28] Z. Zhu, Y. Tian, Y. Liu, K. Fu, Q. Chen, B. Zhang, H. Zhang, Q. Zhang, *Colloids Surf.,A* **2022**, *641*, 128562.
[29] C. Zeng, Y. Shen, J. Tao, H. Chen, Z. Wang, S. Liu, D. Lu, X. Xie, *Langmuir* **2022**, *38*, 937.
[30] K. Golovin, A. Dhyani, M. D. Thouless, A. Tuteja, *Science* **2019**, *364*, 371.
[31] A. Dhyani, C. Pike, J. L. Braid, E. Whitney, L. Burnham, A. Tuteja, *Adv. Mater. Technol.* **2022**, *7*, 2101032.
[32] A. Dhyani, J. Wang, A. K. Halvey, B. Macdonald, G. Mehta, A. Tuteja, *Science* **2021**, *373*, eaba5010.
[33] Y. Zhuo, J. Chen, S. Xiao, T. Li, F. Wang, J. He, Z. Zhang, *Mater. Horiz.* **2021**, *8*, 3266.
[34] P. Wang, Z. Li, Q. Xie, W. Duan, X. Zhang, H. Han, *J. Bionics Eng.* **2021**, *18*, 55.
[35] H. Sojoudi, M. Wang, N. D. Boscher, G. H. McKinley, K. K. Gleason, *Soft Matter* **2016**, *12*, 1938.
[36] X. Zhang, Y. Guo, H. Chen, W. Zhu, P. Zhang, *J. Mater. Chem. A* **2014**, *2*, 9002.
[37] S. Ramakrishna, K. S. S. Kumar, D. Mathew, C. P. R. Nair, *Sci. Rep.* **2015**, *5*, 1.
[38] S. Roh, A. H. Williams, R. S. Bang, S. D. Stoyanov, O. D. Velev, *Nat. Mater.* **2019**, *18*, 1315.
[39] D. Bonn, J. Eggers, J. Indekeu, J. Meunier, *Rev. Mod. Phys.* **2009**, *81*, 739.
[40] S. Ebnesajjad, in *Handbook of Adhesives and Surface Preparation*, Elsevier Inc., Amsterdam; Boston **2011**, pp. 21–30.
[41] U. Stachewicz, F. Hang, A. H. Barber, *Langmuir* **2014**, *30*, 6819.
[42] K. L. Johnson, K. Kendall, A. D. Roberts, *J. Phys. D Appl. Phys.* **1971**, *324*, 301.
[43] A. Alizadeh, M. Yamada, R. Li, W. Shang, S. Otta, S. Zhong, L. Ge, A. Dhinojwala, K. R. Conway, V. Bahadur, A. J. Vinciquerra, B. Stephens, M. L. Blohm, *Langmuir* **2012**, *28*, 3180.
[44] C. Wang, W. Zhang, A. Siva, D. Tiea, K. J. Wynne, *Langmuir* **2014**, *30*, 540.
[45] C. Rin Yu, A. Shanmugasundaram, D. W. Lee, *Appl. Surf. Sci.* **2022**, *583*, 152500.
[46] L. Han, H. Bi, X. Xie, S. Su, P. Mao, L. Sun, *Nanoscale* **2020**, *12*, 17812.
[47] C. Cao, M. Ge, J. Huang, S. Li, S. Deng, S. Zhang, Z. Chen, K. Zhang, S. S. Al-Deyab, Y. Lai, *J. Mater. Chem. A* **2016**, *4*, 12179.
[48] S. Luiso, A. H. Williams, M. J. Petrecca, S. Roh, O. D. Velev, P. S. Fedkiw, *J. Electrochem. Soc.* **2021**, *168*, 020517.
[49] A. H. Williams, S. Roh, A. R. Jacob, S. D. Stoyanov, L. Hsiao, O. D. Velev, *Nat. Commun.* **2021**, *12*, 2834.
[50] L. Wang, R. Wang, J. Wang, T.-S. Wong, *Sci. Adv.* **2020**, *6*, eabb2307.
[51] Y. Liao, R. Wang, A. G. Fane, *J. Membr. Sci.* **2013**, *440*, 77.
[52] X. Wang, B. Ding, J. Yu, M. Wang, *Nano Today* **2011**, *6*, 510.
[53] S. K. Smoukov, T. Tian, N. Vitchuli, S. Gangwal, P. Geisen, M. Wright, E. Shim, M. Marquez, J. Fowler, O. D. Velev, *Adv. Mater.* **2015**, *27*, 2642.